ACS Photonics

Article

pubs.acs.org/journal/apchd5

Enhanced Absorption and <1% Spectrum-and-Angle-Averaged Reflection in Tapered Microwire Arrays

Sisir Yalamanchili,[†,§,□] Hal S. Emmer,[†,□] Katherine T. Fountaine,[‡,#] Christopher T. Chen,[†] Nathan S. Lewis,[‡,§,∥,⊥] and Harry A. Atwater*[,†,§,∥]

[†]Division of Engineering and Applied Sciences, [‡]Division of Chemistry and Chemical Engineering, [§]The Joint Center for Artificial Photosynthesis, [∥]Kavli Nanoscience Institute, and [⊥]Beckman Institute, California Institute of Technology, Pasadena, California 91125, United States

[#]NGNext, Northrop Grumman Aerospace Systems, 1 Space Park Drive, Redondo Beach, California 90278, United States

Supporting Information

ABSTRACT: We report ordered, high aspect ratio, tapered Si microwire arrays that exhibit an extremely low angular (0° to 50°) and spectrally averaged reflectivity of <1% of the incident 400−1100 nm illumination. After isolating the microwires from the substrate with a polymer infill and peel off process, the arrays were found to absorb 89.1% of angular averaged incident illumination (0° to 50°) in the equivalent volume of a 20 μm thick Si planar slab, reaching 99.5% of the classical light trapping limit between 400 and 1100 nm. We explain the broadband absorption by enhancement in coupling to waveguide modes due to the tapered microstructure of the arrays. Time-resolved microwave photoconductivity decay measurements yielded charge-carrier lifetimes of 0.75 μs (more than an order of magnitude higher than vapor−liquid−solid-grown Si microwires) in the tapered microwires, resulting in an implied V_{oc} of 0.655 V. The high absorption and high aspect ratio in these ordered microwire arrays make them an attractive platform for high-efficiency thin-film crystalline Si solar cells and as well as for the photoelectrochemical production of fuels from sunlight.

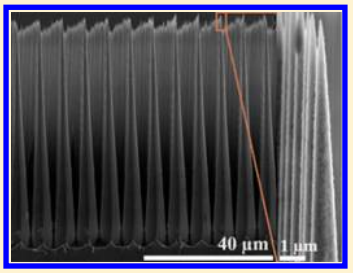

KEYWORDS: *silicon, microwires, reflection, absorption, waveguide, ICPRIE, carrier lifetime, surface passivation*

Reaching toward the ultimate conversion efficiency limits for Si photovoltaics is of considerable fundamental and practical interest and motivates research on thin Si solar cells with high minority carrier lifetimes and extremely efficient light management. While the limiting efficiency[2] for a single-junction crystalline Si solar cell under 1 sun illumination of 29.43% is constrained only by free carrier and Auger absorption losses,[3,4] record experimental Si cells have reached efficiencies as high as 25.6%.[5] To achieve higher efficiencies, lower surface recombination velocities must be achieved in structures with very efficient light management that enable a reduced bulk recombination by virtue of reduced absorber volume in the solar cell. Current high-efficiency Si solar cells utilize intrinsic amorphous silicon (i-a-Si)[6] or Al_2O_3[7] surface passivation layers that produce very low surface recombination velocities, so that the cell performance is typically limited by the bulk carrier lifetime. Consequently, a further decrease in bulk recombination could lead to yet higher cell efficiencies. Heterostructure with intrinsic thin layer (HIT) Si solar cells have demonstrated an efficiency enhancement by the use of thinner substrates.[6] In such HIT cells, the dark current due to recombination is reduced compared to the current under illumination, increasing the quasi-Fermi level. Use of even thinner substrates would be desirable in order to reduce the bulk recombination volume, but the indirect band gap of Si yields reduced absorption in very thin samples. Additionally, the surface/bulk ratio increases as the substrate becomes thinner. The optimal Si cell thickness thus depends strongly on the achievable surface recombination velocities as well as on the ability to achieve enhancements in light trapping. Optoelectronic transport calculations indicate that with realistic surface recombination velocities and high bulk material quality efficiencies as high as 24.4% could be achieved in a 10 μm thick cell[8] if the light trapping were at the $4n^2$ Lambertian limit.[9] It was also suggested that modulated silicon nanowire photonic crystal architectures have the potential to reach 15−20% solar cell efficiencies in only 1 μm equivalent thick silicon.[10] Previous demonstrations of thin-film crystalline Si cells with an effective thickness less than 50 μm with various light -trapping schemes include 20.62% efficiency in a 35 μm device,[5] 19.1% in a 43 μm thick device,[11] 16.8% in a 20 μm thick device,[12] and 15.7%[13] and 13.7%[14] in 10 μm thick devices.

Various nanostructured antireflection and light-trapping strategies have been explored for thin-film crystalline Si.[15,16] Some recent studies have shown limitations in light-trapping structures arising from parasitic absorption, as opposed to limitations in the Si absorber material of the cell. Hence structuring the absorber layer to maximally harvest light while minimizing parasitic absorption and reflection losses is required to maximize absorption in thin crystalline Si solar cells.[17−19] Si microwire arrays facilitate light absorption near the $4n^2$ limit for

Received: May 30, 2016

DOI: 10.1021/acsphotonics.6b00370
ACS Photonics XXXX, XXX, XXX−XXX

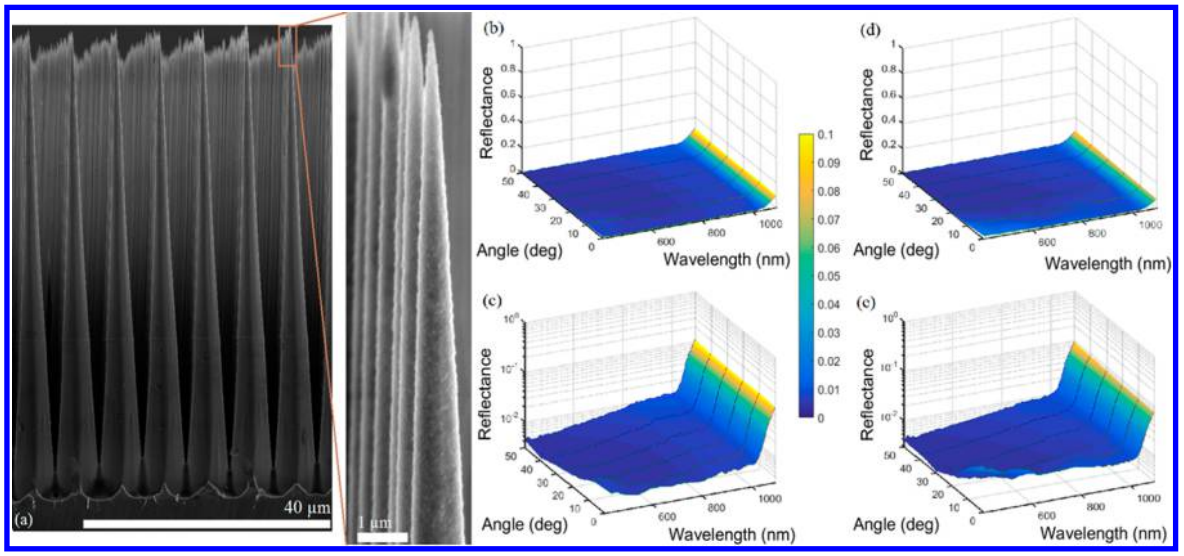

Figure 1. (a) Si substrates with tapered microwire arrays etched via ICPRIE. The inset shows the morphology of the tip of a tapered microwire. (b and c) Reflectance (0.98%) of Si substrates with tapered microwire arrays measured using an integrating sphere plotted on a linear scale and log scale, respectively. (d and e) Reflectance (0.97%) of the arrays with a SiN_x antireflection coating.

very small Si planar equivalent thicknesses,[20] with reports of absorption exceeding the $4n^2$ limit near the band edge. However, to date, Si microwires fabricated by vapor−liquid−solid growth methods using metals such as Au or Cu as growth catalysts have not demonstrated high minority carrier recombination lifetimes, since these metals can produce defects that reduce the bulk recombination lifetime in Si.[1,20,21]

We demonstrate here that Si microwires with high minority carrier bulk lifetimes can be fabricated by cryogenic inductively coupled plasma reactive ion etching (ICPRIE), which is predominantly a chemical etch. The etching conditions can be modified to taper the Si microwire shape to achieve extremely low, angle- and spectrally averaged reflectivity. These arrays were embedded in polydimethylsiloxane (PDMS) and peeled off of their substrate, which can then be reused to etch additional microwire arrays, provided the remaining wafer thickness is sufficient. Such peeled off films exhibited near $4n^2$ light trapping compared to the volumetric equivalent planar Si thin film. Electrodynamic simulations indicate that the tapered Si microwire structure facilitates highly effective coupling of incident light into waveguide modes and yield high optical absorption.

High aspect ratio pillar structures with high precision have been fabricated in Si wafers by a cryogenic ICPRIE for various solid-state device applications.[22] Aluminum oxide (Al_2O_3) is a nearly ideal etch mask with nearly 1:1000 selectivity, which can be used to achieve structures with aspect ratios as high as 20:1.[23] The high aspect ratio tapered microwire arrays shown in Figure 1a are fabricated from high lifetime (>1 ms) float zone grown Si wafers via photolithography followed by ICPRIE and standard Si surface cleaning methods.[24] The resulting structure features wires with a tip radius of curvature of 25 nm, a bottom base diameter of 7 μm, and a height of 75 μm, in a square lattice with 7 μm pitch.

Angle-dependent reflectance measurements were performed using tunable monochromatic radiation from a supercontinuum laser and a Si photodetector.[20] Figure 1b and c show the measured wire array reflectance on linear and log scales, respectively, from 400 to 1100 nm, while the angle was varied from 0° to 50°. Averaged over 0° to 50° and over the range 400−1100 nm, the integrated reflectance was 0.98% for uncoated Si wire arrays and 0.97% for arrays coated with SiN_x dielectric layers. During these measurements no back reflector was employed. The tapered microwire arrays thus act as nearly ideal antireflection surfaces, not only at normal incidence but also at oblique incidence angles even without any antireflection coating. The angular reflectance without and with SiN_x antireflection coating is shown in Figure 1c and d and Figure 1e and f, respectively, in linear and log plots. The surface reflectance is comparable to—and in some cases lower than—typical black Si front-surface texturing methods.[25−27] Notably, low reflection was achieved at wavelengths near the Si band gap, i.e., 1000−1100 nm, where Si has a large absorption length. In the 1000−1100 nm wavelength range, where the absorption depth is on the order of hundreds of micrometers, the reflection varied from 3.6% at normal incidence to 2.7% at 50° for uncoated wires, which is limited by reflection from the back surface of the ∼300 μm thick sample. In the 400−1000 nm range, the reflection varied from 0.7% to 0.5%. Although not all previous work has reported angular averages for reflectance, the present result of <1% angular averaged reflection is to our knowledge a record for low-reflectance silicon structures and compares very favorably to other methods for reducing reflection in the range 400−1100 nm, the wavelength range of interest for Si-based solar cells.

In order to experimentally measure absorption in tapered microwire arrays without effects due to the substrate, the uncoated arrays were embedded in ∼120 μm thick PDMS, by spin coating followed by curing. The arrays were peeled off of their substrate using a razor blade, to produce flexible films with embedded Si microwires.[28,29] The filling ratio of Si/PDMS in these films was ∼1:5. The fill fraction of Si vs height is shown in Figure S4. These films were placed on a nearly ideal Lambertian back-scattering $BaSO_4$ (6080 white reflectance coating; Lab-Sphere)-coated sample holder in an integrating sphere, and reflection (R) measurements were performed. The absorption (A) was calculated from the reflectance (R) data by using $A = 1 - R$. Figure 2a and b show the peeled off PDMS films with embedded, tapered Si microwire arrays. Figure 2c shows the absorption calculated from the reflection measurement in the integrating sphere from 400 to 1100 nm, while the angle was varied from 0° to 50°. Averaged over 0° to 50°, such films showed

DOI: 10.1021/acsphotonics.6b00370
ACS Photonics XXXX, XXX, XXX−XXX

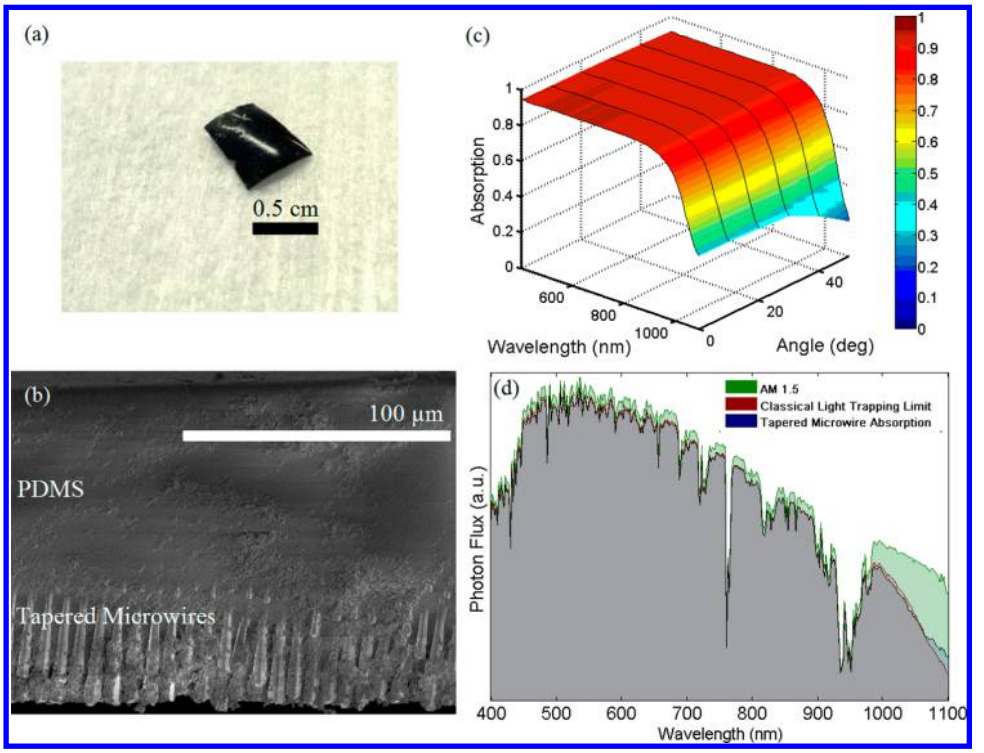

Figure 2. (a) Optical photograph of the films with tapered microwires embedded in PDMS, (b) cross-section SEM of the film, (c) absorption measured in the film in the range 400−1100 nm while varying the angle of incidence from 0° to 50°, and (d) semitransparent area plot for comparison of absorbed photon flux at normal incidence with classical light-trapping limit absorption of a 20 μm thick slab.

an integrated absorbed solar spectrum photon flux as high as 89.1%, demonstrating the remarkable absorption properties of these tapered microwire arrays at various incident angles in the solar spectrum of interest. The effective planar thickness of these polymer-embedded arrays calculated assuming a truncated cone with tip radius of 25 nm, base radius of 3.5 μm, and height of 70 μm is ∼20 μm. Figure 2d shows semitransparent area plots comparing the total incident photon flux (green), absorbed solar flux under normal incidence in tapered microwire arrays embedded in PDMS (blue), and absorption for the $4n^2$ light-trapping limit[30] in a 20 μm thick Si slab, after correcting for reflection from the PDMS/air interface (∼3%) (red). The gray color in the plot indicates the overlap region of all three photon flux plots. The total calculated photon flux absorbed at normal incidence was 99.5% of the limit for an equivalent thick Si slab. Each of the films, fabricated by embedding the tapered microwire arrays in PDMS and peeling the microwires off of their substrate and placed on a nearly ideal Lambertian back reflector, showed absorption slightly below the $4n^2$ limit for most of the solar spectrum and exceeded the limit at wavelengths near the Si band gap (1050−1100 nm).

The exceptionally low reflectivity of the arrays arises from the tapered wire geometry. The fill fraction of the arrays at the light-incident interface is less than 0.01% and linearly increases extremely gradually along the extended length of the tapered microwires to ∼78% at their base. The remarkable optical characteristics—minimal reflection and high absorption—of the tapered Si microwire arrays cannot be completely explained by either the effective medium concept or ray optic analysis especially at wavelengths near the band gap of Si and require a wave-optical analysis for quantification. A previous theoretical study of Si microwire optical properties indicated that ray optical models are insufficient to explain the strong absorption observed experimentally in microwires with radii smaller than 4 μm. The tapered microwires in this study have radii ranging from 50 nm to 3.5 μm. Therefore, we employed full-wave simulations to accurately model the optical properties of the fabricated tapered microwires.[31] From this, the measured absorption is seen in this case to arise from efficient coupling of incident light into waveguide modes in the wires. We employed a combination of full-wave electromagnetic simulations and analytic waveguide analysis to develop an understanding of the array optical properties. The strong symmetry overlap of specific waveguide modes also contributes to the low reflectivity and is discussed in more detail below. Bloch modes, which often result in reflection bands,[32−34] play an insignificant role in these structures due to an interwire spacing that is much larger than the optical wavelength. Consequently, each tapered microwire acts as an independent optical antenna and waveguide, consistent with previous findings.[35−37]

The high absorption arises from a combination of coupling into waveguide modes and the length of the microwires. Many groups have studied and demonstrated enhanced absorption in Si nanowire arrays due to coupling into waveguide modes with large extinction cross sections.[38−42] Owing to nanofabrication-imposed limitations to the achievable nanowire aspect ratio, the Si nanowire array absorption is typically much lower than that for optically thick planar Si absorbers, despite field enhancements due to the material volume required to achieve near-unity absorption in indirect band-gap materials.[43] Our microwire structures also capitalize on waveguide modes for optical absorption enhancement, while simultaneously incorporating long optical path lengths to achieve near-unity absorption. Efficient coupling into the optical waveguide modes of the Si microwires is the critical factor in the remarkable optical properties of these arrays.

DOI: 10.1021/acsphotonics.6b00370
ACS Photonics XXXX, XXX, XXX−XXX

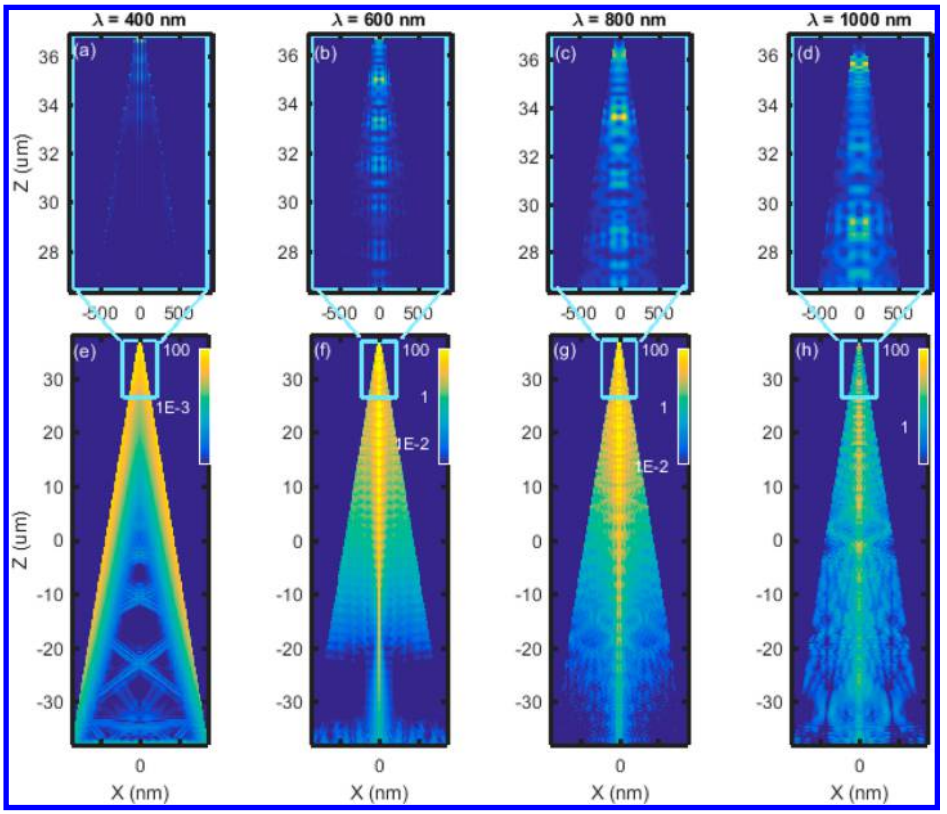

Figure 3. Longitudinal cross sections of power absorption for Si microwires at 400 (a, e), 600 (b, f), 800 (c, g), and 1000 (d, h) nm wavelengths, respectively: (a−d) upper portion of microwire with linear intensity scale; (e−h) complete microwire with logarithmic intensity scale; light blue squares correspond to expanded cross sections in (a)−(d); different relative scales are used for each figure to highlight modes.

Three-dimensional full-field electromagnetic wave simulations of tapered microwire arrays were performed to characterize the waveguide modes. The simulation procedure is explained in detail in the Methods section. Figure 3 displays carrier generation cross sections for tapered microwires at incident wavelengths of 400, 600, 800, and 1000 nm, respectively. Figure 3e−h show complete wire cross sections on a logarithmic scale, marked with light blue squares indicating the bounds of Figure 3a−d, which focus on the upper portion of the wire and are shown in linear scale. All absorption profiles indicate light coupling into waveguide modes, but the modes are less obvious at λ = 400 nm (Figure 3a and e), due to strong absorption above the direct gap of Si. Below the direct gap of Si, the waveguide characteristics become more apparent. Absorption occurs primarily in the microwire core, indicative of guided mode propagation in the wire, and exhibits semiperiodic longitudinal intensity oscillations that scale with incident wavelength; these longitudinal oscillations in field intensity are not representative of any longitudinal interference modes, but rather are indicative of the phase cycle of mode propagation. This distinction is critical because longitudinal interference modes would require long solar coherence lengths, whereas mode propagation does not. Additionally, the existence of significant intensity near the lower end of the microwire in the λ = 1000 nm profile demonstrates long-distance waveguide mode propagation to the bottom of the microwire, enabling near-unity absorption for wavelengths near the Si band edge. Simulations show that the reflection is <1% at wavelengths below 1000 nm, agreeing with the measurements. Since carrier generation was observed to occur predominantly in the upper portion of the wires, the minor deviation from perfectly circular wire shape seen in Figure 1a at the base of the wires is not expected to give rise to a significant change in the optical properties relative to the circular cross sections assumed in our simulations.

Detailed mode analysis reveals that light couples into the set of first azimuthal order waveguide modes, HE_{1n}, as illustrated for λ = 1000 nm illumination in Figure 4. As previously reported,[44,45] efficient coupling occurs into this set of modes due to the strong overlap in symmetry between the incident plane wave and the in-plane mode field profiles. Figure 4a displays a longitudinal cross section marked with horizontal dashed lines colored to indicate their correlation with the radial cross sections in Figure 4b−g; the radial cross sections correspond to the first six HE_{1n} modes, in ascending order. As expected, the first-order HE_{11} mode appears at the top of the wire, and the higher order modes appear in sequence, as the radius increases.

$$\left(\frac{1}{k_{cyl}^2}-\frac{1}{k_{out}^2}\right)^2\left(\frac{\beta m}{k_0 a}\right)^2 = \left(\frac{\varepsilon_{r,cyl}\mu_{r,cyl}}{k_{cyl}}\frac{J_m'(k_{cyl}a)}{J_m(k_{cyl}a)}-\frac{\varepsilon_{r,out}\mu_{r,out}}{k_{out}}\frac{H_m'(k_{out}a)}{H_m(k_{out}a)}\right)\times \left(\frac{1}{k_{cyl}}\frac{J_m'(k_{cyl}a)}{J_m(k_{cyl}a)}-\frac{1}{k_{out}}\frac{H_m'(k_{out}a)}{H_m(k_{out}a)}\right) \quad (1)$$

The dispersion curves for these modes were calculated from the eigenvalue equation (eq 1) for cylindrical dielectric waveguides,[46] where J_m and H_m are the cylindrical Bessel and Hankel functions of the mth order, k_0 is the free-space wavevector, k_{cyl} (k_{out}) is the transverse wavevector inside

DOI: 10.1021/acsphotonics.6b00370
ACS Photonics XXXX, XXX, XXX−XXX

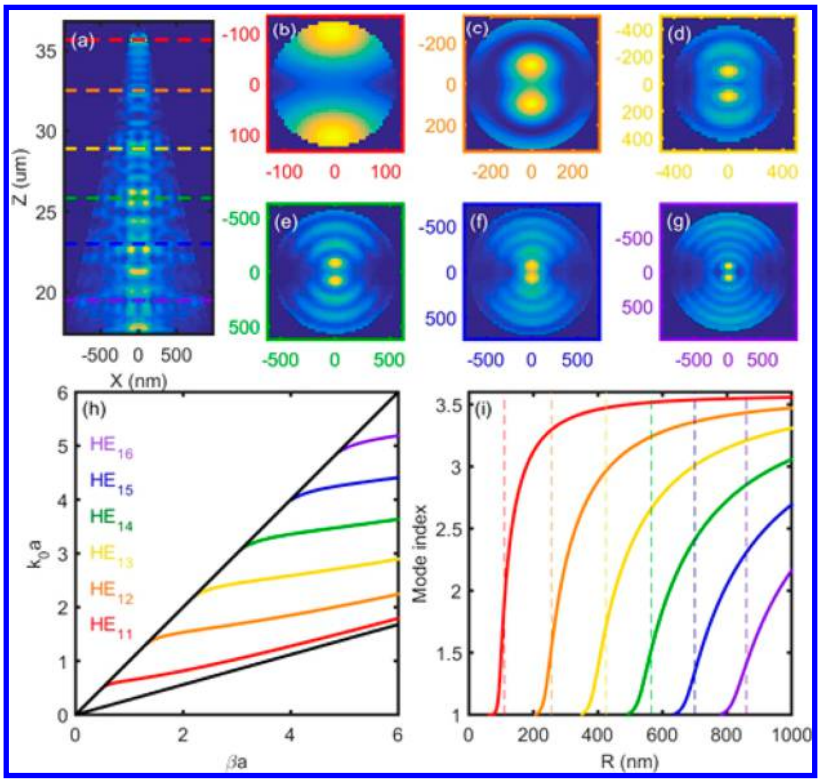

Figure 4. Detailed mode analysis of upper portion of a tapered microwire at λ = 1000 nm; mode color key in (h) is applied throughout the figure: (a) longitudinal absorption cross section with dashed lines indicating radial cross sections; (b–g) radial cross sections, exhibiting HE_{1n} modes; (h) traditional dispersion curves for HE_{1n} modes for n = 3.577; (i) nontraditional dispersion curves, converted from (h) for λ = 1000 nm.

(outside) the cylinder, β is the mode propagation constant, $\varepsilon_{r,cyl}$ ($\varepsilon_{r,out}$) and $\mu_{r,cyl}$ ($\mu_{r,out}$) are the relative dielectric permittivity and permeability inside (outside) the cylinder, and a is the cylinder radius. Figure 4h and i show the dispersion curve for a Si waveguide (n = 3.577), in its traditional form, $k_0a(\beta a)$, and a nontraditional form, mode index vs radius, respectively. The mode color key in Figure 4h is consistent throughout the figure. The dashed lines in Figure 4i indicate the radius of the mode cross sections in Figure 4b–g, revealing that the modes are most prominent between a mode index of 1 and 2. This moderate mode index is due to a trade-off between ease of free-space coupling and mode confinement mediated absorption. Mode profiles, propagation constants, and radius range are all consistent with analytic waveguide theory. These observations demonstrate the critical role of waveguide modes in the optical characteristics of the tapered microwire arrays.

In order to evaluate the quality of tapered microwires and estimate the V_{oc}, transmission electron microscopy (TEM) and lifetime measurements were performed. Electron microscopy images of the sidewall shown in Figure S1 (see Supporting Information) show minimal surface damage due to etching and no lattice damage in the bulk, as expected from the low forward power (5 W) and predominantly chemical nature of the dry etching process. The carrier recombination lifetimes were measured for tapered microwire arrays passivated by Al_2O_3-coated microwires by atomic layer deposition (ALD)[7,47] using a custom-built microwave photoconductive decay lifetime tool with a Nd:YaG laser illumination source operating at 1064 nm. Pulses of 30–240 μJ energy of 5 ns and spot size of 3 mm diameter at 10 Hz frequency were used for these measurements, as illustrated in Figure S2 (see Supporting Information). The cleaning process steps and the measurement technique of these tapered microwires are detailed in the Methods section. Al_2O_3-passivated tapered microwire arrays were embedded in PDMS and peeled from their respective substrates using a razor blade. During the measurements, the fractured back surfaces of the peeled microwires were passivated *in situ* using 5.8 M HCl, after a 20 s damage removal etch in 3.6 M KOH at room temperature. All the lifetime measurements resulted in continuously increasing lifetimes as a function of intensity, indicating that measurements were done at the onset of high injection level.[48] Lifetimes of 0.75 μs were measured in these arrays with 240 μJ pulses. An analytical model was implemented to estimate surface recombination velocity (SRV), implied V_{oc}, and the corresponding maximum limiting efficiency achievable from the carrier lifetime measurements. The SRV achieved was estimated to be 150 cm/s, with the corresponding implied V_{oc} being 0.655 V and the maximum efficiency achievable being 22.2%. The model is described in detail in the Methods section. The tapered microwire arrays are surface recombination limited, and a further decrease in SRV to 5 cm/s is shown to enhance the lifetime to >15 μs and the maximum limiting efficiency to >25%.

In conclusion, the tapered microwire arrays fabricated in this work demonstrate superior light-trapping properties with <1% angular averaged reflection and absorption reaching the $4n^2$ light-trapping limit due to enhanced coupling of incident light into the waveguide modes. The high absorption arises from a combination of coupling into waveguide modes and overall length of the microwires, resulting in absorption that approaches the ray optic light-trapping limit over most of the solar spectrum and absorption above the ray optic limit at wavelengths near the Si energy band gap.[49,50] These microwires show no bulk damage and minimal surface damage that can be removed by surface cleaning after fabrication. We measured carrier lifetime in these

DOI: 10.1021/acsphotonics.6b00370
ACS Photonics XXXX, XXX, XXX–XXX

microstructures by microwave-detected photoconductivity measurement and measured lifetimes of 0.75 μs for wires under ALD-deposited 20 nm thick Al_2O_3 sidewall passivation with 5.8 M HCl back surface passivation. In this work the performance of the arrays is limited by surface recombination, and therefore further improvement in surface passivation methods to these arrays can push the performance of these arrays to reach V_{oc} > 0.7 V and a maximum possible efficiency of >25%. The efficiencies estimated by our model provide the absolute maximum possible limiting values that are in principle achievable given the material volume, surface area of the fabricated structure, and the observed optical properties. The real-world device architectures we envision utilizing these tapered microwire arrays include all back contact solar cells[7,14,47,51] similar to previous demonstrations with an ultrathin Si substrate[52] or as a flexible solar cell with a conventional back contact and a transparent front contact.[29] The effect of resistances in the structures and selective contacts are expected to reduce the estimated efficiency further. In this study, ICPRIE was chosen as the fabrication technique because it offers significant optoelectronic performance advantages: the electronic quality of the bulk wafer is preserved and the fine control over the shape of etched structures enables optimal optical design. Due to the high surface area and superior light trapping, these tapered microwires are also excellent candidates for applications in photoelectrochemical cells and enhancing electrode efficiencies[53−57]

METHODS

Fabrication of Tapered Microwire Arrays. High-lifetime (~1 ms) float zone grown Si wafers were photolithographically patterned into a square grid with 3 μm circles of 200 nm thick Al_2O_3 mask evaporated over it separated by 7 μm. SF_6/O_2 etch chemistry was used in an Oxford DRIE System 100 ICP/RIE to perform the etching. Etching was performed at a low capacitive coupled power of 5 W to reduce damage due to the momentum of the ions. A high inductively coupled power of 900 W was used to increase the number of ions in the plasma to reach high rates of chemical etch. The etch was performed in three steps where the SF_6/O_2 ratio was increased from 70 sccm/5 to 70 sccm/6 sccm in steps of 0.5 sccm of O_2 flow rate every 30 min. The chamber was maintained at a temperature of −120 °C and a pressure of 10 mTorr during the etching process. Post etching, the wafers were dipped in buffered hydrofluoric acid solutions to etch away the Al_2O_3 mask. The resulting tapered microwire arrays are shown in Figure 1a. The bar on the silicon microwires visible at 30 μm from the base of the wires was a result of stopping and starting the plasma during the transition from step 2 with 5.5 sccm O_2 flow rate to step 3 with 6 sccm O_2 flow rate. The samples were then cleaned using modified RCA1 and RCA2 cleaning processes.[24] SiN_x was deposited over the Si wire substrates by plasma-enhanced chemical vapor deposition using an Oxford Instruments Plasmalab System 100. Silane and ammonia gas chemistry was used at 350 °C and 1 Torr at previously optimized conditions for microwire arrays.[20]

Sample Preparation for Absorption Measurements. Tapered microwire arrays were embedded in PDMS by spin coating a 1:1 by weight solution of toluene/PDMS at 500 rpm so that all the wires were completely embedded in PDMS to avoid any damage to the tip while handling. The sample was heated on a hot plate at a temperature of 120 °C for 5 h. The tapered wire arrays embedded in PDMS were peeled off the surface using a razor blade to obtain flexible films as shown in Figure 3a.

Al_2O_3 Atomic Layer Deposition for Lifetime Measurements. Al_2O_3 was deposited over Si by atomic layer deposition using trimethylaluminum and water as precursors at 150 °C. The precursors were pulsed for 15 ms at 20 s intervals for 200 cycles. The Si samples then annealed at 400 °C for 10 min under a nitrogen flow of 3 lpm.

Simulation Procedure for Optical Properties. Rigorous 3D full-field electromagnetic wave FDTD simulations of tapered microwire arrays were performed using a commercial software package, Lumerical FDTD. The arrays were constructed using the 3D rectangular simulation region with periodic boundary conditions along x- and y-axes to depict a 7 μm square lattice of the arrays, and infinite boundary conditions rendered as perfectly matched layers along the z-axis. In the simulation region tapered microwires had a top diameter of 50 nm, bottom diameter of 7 μm, and height of 75 μm. Palik material data provided by Lumerical were used for modeling the material as Si. Single-wavelength infinite plane wave sources at four different wavelengths (400, 600, 800, and 1000 nm) were used with a long pulse time of 50 fs to simulate steady-state behavior. Generation rate in these structures was calculated by using the built-in CW-generation (continuous wave generation) rate analysis group to obtain electron−hole pair generation profiles under steady-state illumination.

Implied V_{oc} and Limiting Efficiency Calculation. The model was implemented in Microsoft Excel, using VBA to iteratively solve the transcendental equations for steady-state carrier concentration. Equivalent planar thickness, surface area, total absorption, surface recombination velocity, radiative recombination coefficient, Shockley−Reed−Hall coefficients,[58] and Auger recombination coefficients[59] in the bulk were input parameters. This model gives the absolute theoretical *maximum* limiting V_{oc} and efficiency that can be achieved in principle from the tapered microwire light-trapping structures with the measured lifetimes. The average steady-state excess carrier concentration was obtained by solving for equivalence of the total generation rate and sum of all recombination rates due to the four recombination mechanisms considered. In this model we ignored the effects of resistances and assumed a narrow selective contact; therefore the change in quasi Fermi levels in the bulk of Si is very small. The quasi Fermi level separation and maximum V_{oc} achievable are obtained from eq 2. To estimate the total carrier generation, an internal quantum efficiency of 100% was assumed, and the total photon flux absorbed was calculated from the measured absorption in tapered microwire arrays under an AM 1.5 spectrum. Because the etching process was predominantly chemical and no bulk damage was observed in TEM analysis, the bulk lifetime was assumed to be 1 ms (same as the lifetime measured in the starting wafer into which the structures were etched). Finally, an efficiency was extracted using the total generation as the J_{sc} and calculating a fill factor using the empirical model for a device without series resistance or shunting developed by M. A. Green.[60] In this model an intrinsic doping density (n_i) of 9.7×10^9 cm^{-3}, donor doping density (N_d) of 10^{17} cm^{-3}, and radiative recombination coefficient (B_{rad}) of 4.7×10^{15} cm^3 s^{-1} were used. This model provides an estimate for the absolute maximum achievable efficiency. In realistic photovoltaic devices, resistances are expected to reduce the efficiencies relative to those calculated via this model.

$$V_{oc} = E_{fn} - E_{fp} = \frac{kT}{q}\ln\left(\frac{(N_A + \Delta n)\Delta n}{n_i^2}\right) \quad (2)$$

DOI: 10.1021/acsphotonics.6b00370
ACS Photonics XXXX, XXX, XXX−XXX

■ ASSOCIATED CONTENT

Supporting Information

The Supporting Information is available free of charge on the ACS Publications website at DOI: 10.1021/acsphotonics.6b00370.

More details regarding TEM, microwave photoconductivity decay (MW-PCD) setup, and fill fraction of samples used for optical and lifetime measurements (PDF)

■ AUTHOR INFORMATION

Corresponding Author

*E-mail (H. A. Atwater): haa@caltech.edu.

Author Contributions

□S. Yalamanchili and H. S. Emmer contributed equally.

Notes

The authors declare no competing financial interest.

■ ACKNOWLEDGMENTS

This work was supported in part by the National Science Foundation (NSF) and the Department of Energy (DOE) under NSF CA No. EEC-1041895 (H.S.E. and C.T.C.) and Joint Center for Artificial Photosynthesis, a DOE Energy Innovation Hub, supported through the Office of Science of the U.S. Department of Energy under Award No. DE- SC0004993. Some of us (C.T.C., H.A.A.) are also supported in part by the U.S. Department of Energy through the Bay Area Photovoltaic Consortium under Award Number DE-EE0004946. We thank Dennis Friedrich for his collaborations for microwave-detected photoconductive decay measurements, Prof. Shu Hu for stimulating discussions, and Carol Garland for her assistance with TEM. This work benefited from use of the Applied Physics and Materials Science Department's Transmission Electron Microscopy Facility. Fabrication was performed in Kavli Nanoscience Institute (KNI) at Caltech, and we thank KNI staff for their assistance during fabrication. Lumerical FDTD simulations for this research used resources of the National Energy Research Scientific Computing Center, a DOE Office of Science User Facility supported by the Office of Science of the U.S. Department of Energy under Contract No. DE-AC02-05CH11231.

■ REFERENCES

(1) Putnam, M. C.; Turner-Evans, D. B.; Kelzenberg, M. D.; Boettcher, S. W.; Lewis, N. S.; Atwater, H. A. 10 μm minority-carrier diffusion lengths in Si wires synthesized by Cu-catalyzed vapor-liquid-solid growth. *Appl. Phys. Lett.* **2009**, *95*, 163116.

(2) Shockley, W.; Queisser, H. J. Detailed Balance Limit of Efficiency of p-n Junction Solar Cells. *J. Appl. Phys.* **1961**, *32*, 510−519.

(3) Tiedje, T.; Yablonovitch, E.; Cody, G. D.; Brooks, B. G. Limiting efficiency of silicon solar cells. *IEEE Trans. Electron Devices* **1984**, *31*, 711−716.

(4) Richter, A.; Glunz, S. W.; Werner, F.; Schmidt, J.; Cuevas, A. Improved quantitative description of Auger recombination in crystalline silicon. *Phys. Rev. B: Condens. Matter Mater. Phys.* **2012**, *86*, 165202.

(5) Green, M. A.; Emery, K.; Hishikawa, Y.; Warta, W.; Dunlop, E. D. Solar cell efficiency tables (version 47). *Prog. Photovoltaics* **2016**, *24*, 3−11.

(6) Taguchi, M.; Yano, A.; Tohoda, S.; Matsuyama, K.; Nakamura, Y.; Nishiwaki, T.; Fujita, K.; Maruyama, E. 24.7% Record Efficiency HIT Solar Cell on Thin Silicon Wafer. *Photovoltaics, IEEE Journal of* **2014**, *4*, 96−99.

(7) Ortega, P.; Calle, E.; von Gastrow, G.; Repo, P.; Carrió, D.; Savin, H.; Alcubilla, R. High-efficiency black silicon interdigitated back contacted solar cells on p-type and n-type c-Si substrates. *Prog. Photovoltaics* **2015**, *23*, 1448−1457.

(8) Kowalczewski, P.; Bozzola, A.; Liscidini, M.; Claudio Andreani, L. Light trapping and electrical transport in thin-film solar cells with randomly rough textures. *J. Appl. Phys.* **2014**, *115*, 194504.

(9) Yablonovitch, E. Statistical ray optics. *J. Opt. Soc. Am.* **1982**, *72*, 899−907.

(10) Deinega, A.; John, S. Solar power conversion efficiency in modulated silicon nanowire photonic crystals. *J. Appl. Phys.* **2012**, *112*, 074327.

(11) Brendel, R.; Petermann, J. H.; Zielke, D.; Schulte-Huxel, H.; Kessler, M.; Gatz, S.; Eidelloth, S.; Bock, R.; Rojas, E. G.; Schmidt, J.; Dullweber, T.; High-Efficiency Cells; From Layer; Transfer, A. First Step Toward Thin-Film/Wafer Hybrid Silicon Technologies. *IEEE J. Photovoltaics* **2011**, *1*, 9−15.

(12) Wang, L.; Lochtefeld, A.; Han, J.; Gerger, A. P.; Carroll, M.; Ji, J.; Lennon, A.; Li, H.; Opila, R.; Barnett, A. Development of a 16.8% Efficient 18-μm Silicon Solar Cell on Steel. *IEEE Journal of Photovoltaics* **2014**, *4*, 1397−1404.

(13) Branham, M. S.; Hsu, W.-C.; Yerci, S.; Loomis, J.; Boriskina, S. V.; Hoard, B. R.; Han, S. E.; Chen, G. Silicon Solar Cells: 15.7% Efficient 10-μm-Thick Crystalline Silicon Solar Cells Using Periodic Nanostructures (Adv. Mater. 13/2015). *Adv. Mater.* **2015**, *27*, 2268−2268.

(14) Jeong, S.; McGehee, M. D.; Cui, Y. All-back-contact ultra-thin silicon nanocone solar cells with 13.7% power conversion efficiency. *Nat. Commun.* **2013**, *4*.10.1038/ncomms3950

(15) Brongersma, M. L.; Cui, Y.; Fan, S. Light management for photovoltaics using high-index nanostructures. *Nat. Mater.* **2014**, *13*, 451−460.

(16) Raut, H. K.; Ganesh, V. A.; Nair, A. S.; Ramakrishna, S. Anti-reflective coatings: A critical, in-depth review. *Energy Environ. Sci.* **2011**, *4*, 3779−3804.

(17) Berginski, M.; Hüpkes, J.; Gordijn, A.; Reetz, W.; Wätjen, T.; Rech, B.; Wuttig, M. Experimental studies and limitations of the light trapping and optical losses in microcrystalline silicon solar cells. *Sol. Energy Mater. Sol. Cells* **2008**, *92*, 1037−1042.

(18) Jovanov, V.; Planchoke, U.; Magnus, P.; Stiebig, H.; Knipp, D. Influence of back contact morphology on light trapping and plasmonic effects in microcrystalline silicon single junction and micromorph tandem solar cells. *Sol. Energy Mater. Sol. Cells* **2013**, *110*, 49−57.

(19) Depauw, V.; Meng, X.; Daif, O. E.; Gomard, G.; Lalouat, L.; Drouard, E.; Trompoukis, C.; Fave, A.; Seassal, C.; Gordon, I. Micrometer-Thin Crystalline-Silicon Solar Cells Integrating Numerically Optimized 2-D Photonic Crystals. *IEEE J. Photovoltaics* **2014**, *4*, 215−223.

(20) Putnam, M. C.; Boettcher, S. W.; Kelzenberg, M. D.; Turner-Evans, D. B.; Spurgeon, J. M.; Warren, E. L.; Briggs, R. M.; Lewis, N. S.; Atwater, H. A. Si microwire-array solar cells. *Energy Environ. Sci.* **2010**, *3*, 1037−1041.

(21) Kelzenberg, M. D.; Turner-Evans, D. B.; Putnam, M. C.; Boettcher, S. W.; Briggs, R. M.; Baek, J. Y.; Lewis, N. S.; Atwater, H. A. High-performance Si microwire photovoltaics. *Energy Environ. Sci.* **2011**, *4*, 866−871.

(22) Shearn, M.; Sun, X.; Henry, M. D.; Yariv, A.; Scherer, A. Advanced Plasma Processing: Etching, Deposition, and Wafer Bonding Techniques for Semiconductor Applications. In *Semiconductor Technologies*; Grym, J., Ed.; InTech, 2010; pp 79−104.

(23) Henry, M. D.; Walavalkar, S.; Homyk, A.; Scherer, A. Alumina etch masks for fabrication of high-aspect-ratio silicon micropillars and nanopillars. *Nanotechnology* **2009**, *20*, 255305.

(24) Kern, W.; Puotinen, A. A. Cleaning Solutions Based on Hydrogen Peroxide for Use in Silicon Semiconductor Technology. *RCA Rev.* **1970**, *31*, 187−206.

(25) Liu, X.; Coxon, P. R.; Peters, M.; Hoex, B.; Cole, J. M.; Fray, D. J. Black silicon: fabrication methods, properties and solar energy applications. *Energy Environ. Sci.* **2014**, *7*, 3223−3263.

(26) Sainiemi, L.; Jokinen, V.; Shah, A.; Shpak, M.; Aura, S.; Suvanto, P.; Franssila, S. Non-Reflecting Silicon and Polymer Surfaces by Plasma Etching and Replication. *Adv. Mater.* **2011**, *23*, 122−126.

DOI: 10.1021/acsphotonics.6b00370
ACS Photonics XXXX, XXX, XXX−XXX

(27) Cho, S. J.; An, T.; Lim, G. Three-dimensionally designed anti-reflective silicon surfaces for perfect absorption of light. *Chem. Commun.* **2014**, *50*, 15710−15713.
(28) Plass, K. E.; Filler, M. A.; Spurgeon, J. M.; Kayes, B. M.; Maldonado, S.; Brunschwig, B. S.; Atwater, H. A.; Lewis, N. S. Flexible Polymer-Embedded Si Wire Arrays. *Adv. Mater.* **2009**, *21*, 325−328.
(29) Turner-Evans, D. B.; Emmer, H.; Chen, C. T.; Atwater, H. A. Flexible, Transparent Contacts for Inorganic Nanostructures and Thin Films. *Adv. Mater.* **2013**, *25*, 4018−4022.
(30) Akimov, Y. A.; Koh, W. S.; Ostrikov, K. Enhancement of optical absorption in thin-film solar cells through the excitation of higher-order nanoparticle plasmon modes. *Opt. Express* **2009**, *17*, 10195−10205.
(31) Kosten, E. D.; Warren, E. L.; Atwater, H. A. Ray optical light trapping in silicon microwires: exceeding the 2n2 intensity limit. *Opt. Express* **2011**, *19*, 3316−3331.
(32) Chow, E.; Lin, S. Y.; Johnson, S. G.; Villeneuve, P. R.; Joannopoulos, J. D.; Wendt, J. R.; Vawter, G. A.; Zubrzycki, W.; Hou, H.; Alleman, A. Three-dimensional control of light in a two-dimensional photonic crystal slab. *Nature* **2000**, *407*, 983.
(33) Joannopoulos, J. D.; Villeneuve, P. R.; Fan, S. Photonic crystals: putting a new twist on light. *Nature* **1997**, *386*, 143−149.
(34) Joannopoulos, J. D.; Johnson, S. G.; Winn, J. N.; Meade, R. D. *Photonic Crystals: Molding the Flow of Light*, 2nd ed.; Princeton University Press: Princeton, 2008.
(35) Fountaine, K. T.; Kendall, C. G.; Atwater, H. A. Near-unity broadband absorption designs for semiconducting nanowire arrays via localized radial mode excitation. *Opt. Express* **2014**, *22*, A930−A940.
(36) Grzela, G.; Paniagua-Domínguez, R.; Barten, T.; Fontana, Y.; Sánchez-Gil, J. A.; Gómez Rivas, J. Nanowire antenna emission. *Nano Lett.* **2012**, *12*, 5481−5486.
(37) Cao, L.; Fan, P.; Vasudev, A. P.; White, J. S.; Yu, Z.; Cai, W.; Schuller, J. A.; Fan, S.; Brongersma, M. L. Semiconductor nanowire optical antenna solar absorbers. *Nano Lett.* **2010**, *10*, 439−445.
(38) Fountaine, K. T.; Whitney, W. S.; Atwater, H. A. Ieee, Achieving Near-Unity Broadband Absorption in Sparse Arrays of GaAs NWs via a Fundamental Understanding of Localized Radial Modes. *Ieee 40th Photovoltaic Specialist Conference (Pvsc)* **2014**, 3507−3509.
(39) Fountaine, K. T.; Whitney, W. S.; Atwater, H. A. Resonant absorption in semiconductor nanowires and nanowire arrays: Relating leaky waveguide modes to Bloch photonic crystal modes. *J. Appl. Phys.* **2014**, *116*, 6.
(40) Garnett, E.; Yang, P. D. Light Trapping in Silicon Nanowire Solar Cells. *Nano Lett.* **2010**, *10*, 1082−1087.
(41) Cao, L. Y.; White, J. S.; Park, J. S.; Schuller, J. A.; Clemens, B. M.; Brongersma, M. L. Engineering light absorption in semiconductor nanowire devices. *Nat. Mater.* **2009**, *8*, 643−647.
(42) Dasog, M.; Carim, A. I.; Yalamanchili, S.; Atwater, H. A.; Lewis, N. S. Profiling Photoinduced Carrier Generation in Semiconductor Microwire Arrays via Photoelectrochemical Metal Deposition. *Nano Lett.* **2016**, *16*, 5015−5021.
(43) Hu, L.; Chen, G. Analysis of Optical Absorption in Silicon Nanowire Arrays for Photovoltaic Applications. *Nano Lett.* **2007**, *7*, 3249−3252.
(44) Abujetas, D. R.; Paniagua-Dominguez, R.; Sanchez-Gil, J. A. Unraveling the Janus Role of Mie Resonances and Leaky/Guided Modes in Semiconductor Nanowire Absorption for Enhanced Light Harvesting. *ACS Photonics* **2015**, *2*, 921−929.
(45) Anttu, N.; Xu, H. Q. Coupling of Light into Nanowire Arrays and Subsequent Absorption. *J. Nanosci. Nanotechnol.* **2010**, *10*, 7183−7187.
(46) Love, A. W. S. J. *Optical Waveguide Theory*; Spring Science & Business Media, 2012.
(47) Savin, H.; Repo, P.; von Gastrow, G.; Ortega, P.; Calle, E.; Garín, M.; Alcubilla, R. Black silicon solar cells with interdigitated back-contacts achieve 22.1% efficiency. *Nat. Nanotechnol.* **2015**, *10*, 624−628.
(48) Rein, S. Lifetime measurement techniques. In *Lifetime Spectroscopy - A method of defect characterization in silicon for photovoltaic applications*; Springer: Germany, 2005; pp 59−68.
(49) Yu, Z.; Raman, A.; Fan, S. Fundamental limit of nanophotonic light trapping in solar cells. *Proc. Natl. Acad. Sci. U. S. A.* **2010**, *107*, 17491−17496.
(50) Callahan, D. M.; Munday, J. N.; Atwater, H. A. Solar Cell Light Trapping beyond the Ray Optic Limit. *Nano Lett.* **2012**, *12*, 214−218.
(51) Kerschaver, E. V.; Beaucarne, G. Back-contact solar cells: a review. *Prog. Photovoltaics* **2006**, *14*, 107−123.
(52) Wang, S.; Weil, B. D.; Li, Y.; Wang, K. X.; Garnett, E.; Fan, S.; Cui, Y. Large-Area Free-Standing Ultrathin Single-Crystal Silicon as Processable Materials. *Nano Lett.* **2013**, *13*, 4393−4398.
(53) Ardo, S.; Park, S. H.; Warren, E. L.; Lewis, N. S. Unassisted solar-driven photoelectrosynthetic HI splitting using membrane-embedded Si microwire arrays. *Energy Environ. Sci.* **2015**, *8*, 1484−1492.
(54) Boettcher, S. W.; Warren, E. L.; Putnam, M. C.; Santori, E. A.; Turner-Evans, D.; Kelzenberg, M. D.; Walter, M. G.; McKone, J. R.; Brunschwig, B. S.; Atwater, H. A.; Lewis, N. S. Photoelectrochemical Hydrogen Evolution Using Si Microwire Arrays. *J. Am. Chem. Soc.* **2011**, *133*, 1216−1219.
(55) Maiolo, J. R.; Kayes, B. M.; Filler, M. A.; Putnam, M. C.; Kelzenberg, M. D.; Atwater, H. A.; Lewis, N. S. High Aspect Ratio Silicon Wire Array Photoelectrochemical Cells. *J. Am. Chem. Soc.* **2007**, *129*, 12346−12347.
(56) Walter, M. G.; Warren, E. L.; McKone, J. R.; Boettcher, S. W.; Mi, Q.; Santori, E. A.; Lewis, N. S. Solar Water Splitting Cells. *Chem. Rev.* **2010**, *110*, 6446−6473.
(57) Warren, E. L.; Atwater, H. A.; Lewis, N. S. Silicon Microwire Arrays for Solar Energy-Conversion Applications. *J. Phys. Chem. C* **2014**, *118*, 747−759.
(58) Shockley, W.; Read, W. T. Statistics of the Recombinations of Holes and Electrons. *Phys. Rev.* **1952**, *87*, 835−842.
(59) Auger, P. Sur les rayons β secondaires produits dans un gaz par des rayons X. *C.R.A.S* **1923**, 177.
(60) Green, M. A. Accuracy of analytical expressions for solar cell fill factors. *Sol. Cells* **1982**, *7*, 337−340.

DOI: 10.1021/acsphotonics.6b00370
ACS Photonics XXXX, XXX, XXX−XXX